EUROREGIO BNAM2022
Joint Acoustics Conference
9th-11th of May, Aalborg, Denmark

Simulation of the sound field behind diffractors

Wolfram Bartolomaeus*, Ralf Becker, Fabio Strigari

Section Environmental Protection, Immissions, Federal Highway Research Institute, Bergisch Gladbach, Germany.

*Bartolomaeus@bast.de

Abstract

In analogy to optical reflection gratings, acoustic diffractors cause an upward diffraction of the sound due to their periodic structure. They can be recessed in the roadside space or mounted on a noise barrier. The prerequisite for their effectiveness, the coherence of the incident sound, is fulfilled for passing vehicles at small angular differences and not too high frequencies. By using chambers of different depths, a spectral broadband effect of the diffractors is achieved.

Based on the results presented at Euroregio/BNAM 2022 in the article "Measurements of the acoustic effectiveness of diffractors", the question arises how the acoustic effect of diffractors could be taken into account in the calculation of sound propagation from roads. For this purpose, the propagation of traffic noise over flat terrain described by Rasmussen already in 1982 was extended with an impedance jump road - grassland and applied to the situation with diffractors. By comparing the sound signals of pass-by measurements recorded at different positions, it should be possible to model the acoustic effect of an additional strip of diffractors placed next to the road by a corresponding strip with a frequency-dependent acoustic impedance.

The transformation of the results obtained here into the purely energetic approach of ISO 9613-2 for sound propagation outdoors is certainly not easy. An indirect possibility would be the introduction of a frequency-dependent vertical directivity of the sound sources, which takes the effect of the diffuser into account.

Keywords: diffractor, propagation.

1 Introduction

In 2019 we first noticed the product WHIS®stone of the Dutch company 4Silence. The possibility to reduce road traffic noise by a periodic grid structures with resonance chambers was already known, e.g. from the EU-project HOSANNA (Holistic and sustainable abatement of noise by optimized combinations of natural and artificial means) conducted from 2009 to 2013. But with WHIS®stone a product is available to be practically used for noise abatement at minor roads.

In the supplementary regulation for noise in the Environment Act, published in the Government Gazette of the Netherlands on March 26th 2021 [1], the diffractor is already considered. In the appendix IV the acoustical effect of the diffractor is defined and how to integrate such a device in the Dutch calculation method. But how to include a diffractor in a more general noise propagation method like ISO 1913-2 [2]?

2 Theory

The theory outlined here is for the purpose of understanding the underlining principles in modelling the sound propagation above ground. It is far from completeness.

2.1. Impedance

The impedance of a surface like a ground or a wall $\underline{Z}_W$ is defined as quotient of sound pressure $\underline{p}$ and velocity $\underline{v}$ at the surface

$$\underline{Z}_W := \frac{\underline{p}}{\underline{v}}\bigg|_{surface} \tag{1}$$

The acoustical behaviour of ground is characterised best by the normalised admittance $\underline{\beta}$ as the quotient of the characteristic acoustic impedance of the fluid $Z_0 = \rho_0 c_0$ with density ρ_0 and velocity c_0 and the surface impedance $\underline{Z}_W$

$$\underline{\beta} := \frac{Z_0}{\underline{Z}_W} \tag{2}$$

In the sound propagation model NORD2000 [3] the flow resistivity of ground is classified in seven impedance classes, based on a measuring procedure of Nordtest [4].

In Figure 1 real and imaginary part of the normalised admittance are shown for impedance classes A to G of NORD2000 in the frequency range from 50 Hz to 10 kHz, following the Darcy model, described by Taraldsen in [5].

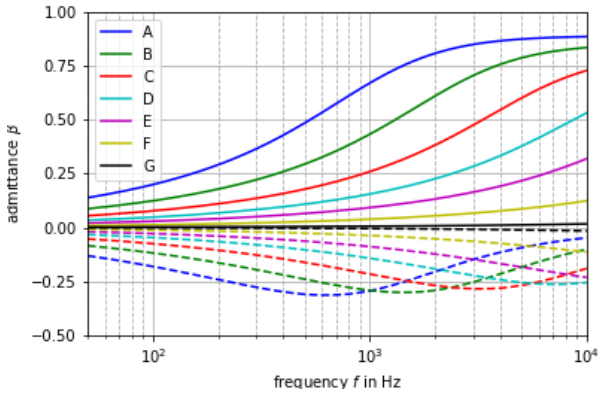

Figure 1: normalised admittance for impedance classes A to G of NORD2000 depending on frequency; solid line: real part, dashed line: imaginary part

The impedance is getting acoustically harder from class A to G. Accordingly, the admittance decreases and the maximum of real and imaginary part of the admittance is moving to higher frequencies. Class "C" is referred as "rough grassland" with flow resistivity of 100 KNs/m^4 while Class "G" corresponds to a hard surface of "dense asphalt" or "concrete" with flow resistivity of 20 000 KNs/m^4.

2.2. Noise propagation above surface

In [6] Nobile the sound propagation over an impedance plane is described. The problem can be solved in cylindrical coordinates. A point source is located in the height of h_Q above a plane with the normalised admittance of $\underline{\beta}$. A receiver is located in a distance of d in the height of h_E above this plane (see Figure 2).

From this, the radial distances between source and receiver, R_1, and between mirror source and receiver, R_2, can be determined.

$$R_1 = \sqrt{(h_E - h_Q)^2 + d^2} \tag{3}$$

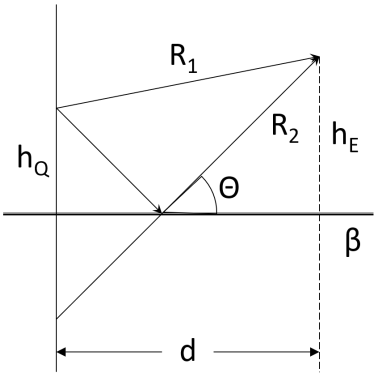

Figure 2: Geometry for the propagation above an impedance plane

$$R_2 = \sqrt{(h_E + h_Q)^2 + d^2} \tag{4}$$

The glancing angle Θ — complementary angle to $\pi/2$ — has the value

$$\Theta = \arctan\left(\frac{d}{h_E + h_Q}\right) \tag{5}$$

The velocity potential with angular wave number k above a local reacting impedance plane (impedance independent of incident angle) is describe by summation of the velocity potentials $\underline{\Psi}_0(R) = nicefrac{e^{ikR}}{R}$ of two spherical sound waves

$$\underline{\Psi}(R_1, R_2) = \underline{\Psi}_0(R_1) + \underline{Q}\underline{\Psi}_0(R_2) = \frac{e^{ikR_1}}{R_1} + \underline{Q}\frac{e^{ikR_2}}{R_2} \tag{6}$$

The spherical reflection factor $\underline{Q}$ is defined by the reflection factor $\underline{R}_p$ of a plane wave and the ground wave function $\underline{F}$

$$\underline{Q} := \underline{R}_p + \left(1 - \underline{R}_p\right)\underline{F} \tag{7}$$

For a sound source near the ground the curvature of the spherical wave has a big influence on reflection. In some cases there is no destructive interference but a ground wave is starting to propagate near the ground.

The ground wave function is defined as

$$\underline{F} := 1 + \mathrm{i}\sqrt{\pi}\underline{w}e^{-\underline{w}^2}\,\underline{\mathrm{erfc}}\left(-\mathrm{i}\underline{w}\right) \tag{8}$$

with the numerical distance

$$\underline{w} := \sqrt{\frac{\mathrm{i}kR_2}{2}}\left(\cos\theta + \underline{\beta}\right) \tag{9}$$

and the complementary error function $\underline{\mathrm{erfc}}$.

The sound pressure of an harmonic point source can be derived from the time deviation of the velocity potential, equation (6), multiplied by the density of the fluid.

In Figure 3 the sound pressure level over an impedance plane of class ”C” of NORD2000 at 1000 Hz is shown for a range of 400 m width and 400 m height.

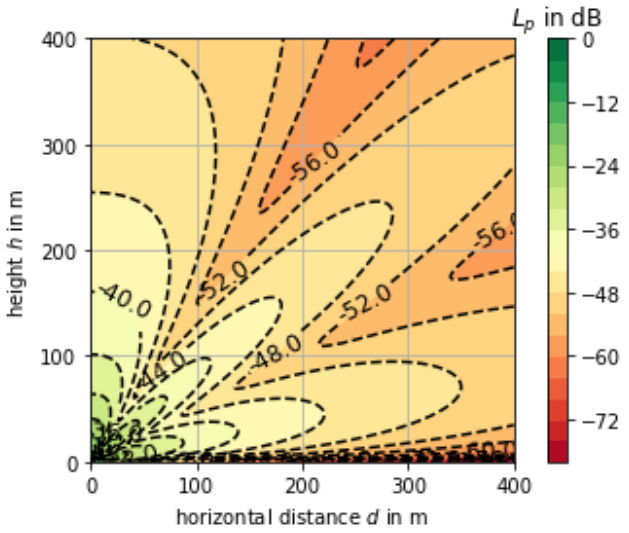

Figure 3: Sound pressure level over an impedance plane of class ”C” at 1000 Hz

The source height was 0.5 m and the source strength was normalised to 0 dB at 1 m distance for free field conditions.

Depending on the impedance of the ground, radial structures of level minima and maxima, originating at the source, occur in the sound field.

2.3. Model with an impedance jump

Rasmussen [7] described a method, developed by de Jong [8] for sound propagation over a plane with an impedance jump. The geometry is displayed in Figure 4.

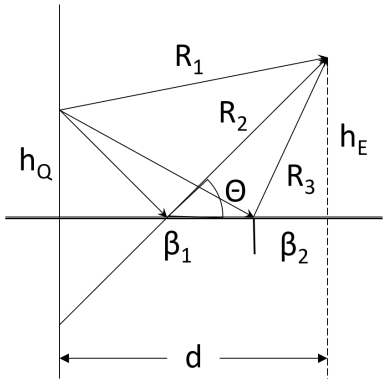

Figure 4: Geometry of sound propagation over an impedance jump

The specular (direct) reflection occurs at the front half plane with admittance β_1.

Beside direct sound and reflection at the impedance plane, corresponding to equation (6) an additional correction term for the velocity potential of the reflection from the impedance jump is introduced

$$\underline{\Psi}_{S\pm} = \frac{e^{-\mathrm{i}\pi/4}}{\sqrt{\pi}} \left[\frac{e^{\mathrm{i}kR_1}}{4\pi R_3} \underline{H}\left(k\sqrt{R_3 - R_1}\right) \pm \frac{e^{\mathrm{i}kR_2}}{4\pi R_3} \underline{H}\left(k\sqrt{R_3 - R_2}\right) \right] \tag{10}$$

The auxiliary function $\underline{H}(x)$ can be expressed by the complex complementary error function

$$\underline{H}(x) = \frac{\sqrt{\pi}}{2} \frac{1+\mathrm{i}}{\sqrt{2}} \underline{\mathrm{erfc}}\left(\frac{1-\mathrm{i}}{\sqrt{2}} x\right) \tag{11}$$

There are two times two cases for the equations. Reflection in the front (1) or in the rear (2) half plane. Impedance of the front half plane is acoustically harder (<) or softer (>) than the rear half plane. For these four cases the equations are

$$\begin{aligned}
1<: \quad \underline{\Psi}_{S,1<} &= \underline{\Psi}_0(R_1) + \underline{Q}_1 \underline{\Psi}_0(R_2) + \left(\underline{Q}_2 - \underline{Q}_1\right) \underline{\Psi}_{S+} \\
1>: \quad \underline{\Psi}_{S,1>} &= \underline{\Psi}_0(R_1) + \underline{Q}_1 \underline{\Psi}_0(R_2) - \left(\underline{Q}_2 - \underline{Q}_1\right) \underline{\Psi}_{S-} \\
2<: \quad \underline{\Psi}_{S,2<} &= \underline{\Psi}_0(R_1) + \underline{Q}_2 \underline{\Psi}_0(R_2) + \left(\underline{Q}_2 - \underline{Q}_1\right) \underline{\Psi}_{S-} \\
2>: \quad \underline{\Psi}_{S,2>} &= \underline{\Psi}_0(R_1) + \underline{Q}_2 \underline{\Psi}_0(R_2) + \left(\underline{Q}_2 - \underline{Q}_1\right) \underline{\Psi}_{S+}
\end{aligned}$$

In Figure 5 the sound pressure level over an impedance plane of class ”G” until 2 m and class ”C” behind at 1000 Hz is shown for a range of 5 to 50 m width and 1 to 5 m height.

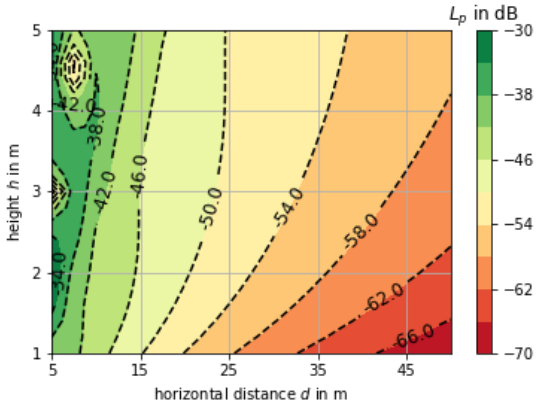

Figure 5: Sound pressure level over an impedance plane of class ”G” until 2 m and class ”C” behind at 1000 Hz

The source height was 0.5 m again and the source strength was normalised to 0 dB at 1 m distance for free field conditions.

At long distance and low height the sound level takes its minimum. At short distance the sound level gets maximum values. This can be assumed as a typical sound field for the radiation of sound from traffic on a road over grassland nearby.

2.4. Modell with two impedance jumps

Hothersall [9] has extended the method of de Jong for a stripe with a different impedance included in the impedance plane. This method can be expanded further for two impedance jumps where all areas are having different impedances. The geometry is shown in Figure 6.

Beside direct sound and specular reflected sound, according equation (6) with a correction for reflection on the first impedance jump according to equation (10) an additional correction term $\underline{\Psi}_{S2\pm}$ for the reflection at the second impedance jump is introduced. For this, in equation (10) the difference between the spherical reflection factors of the two first impedances $\left(\underline{Q}_2 - \underline{Q}_1\right)$ is substituted by the difference of the two last impedances $\left(\underline{Q}_3 - \underline{Q}_2\right)$ and instead of the distance R_{S1} the distance R_{S2} is used.

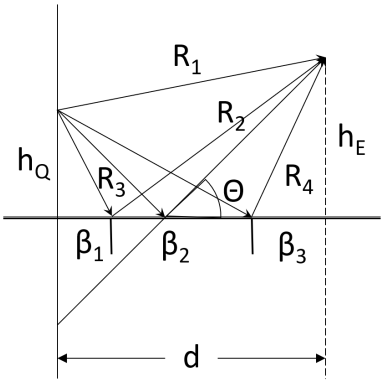

Figure 6: Geometry for sound propagation over an plane with two impedance jumps

Depending on whether the specular reflection occurs in section 1, 2 or 3 and which admittances β_1, β_2 and β_3 in these sections are existent:

$$\begin{aligned}
&\text{a:} \quad |\beta_1| \leq |\beta_2| \leq |\beta_3| \\
&\text{b:} \quad |\beta_1| \leq |\beta_2| \wedge |\beta_2| > |\beta_3| \\
&\text{c:} \quad |\beta_1| > |\beta_2| \wedge |\beta_2| \leq |\beta_3| \\
&\text{d:} \quad |\beta_1| > |\beta_2| > |\beta_3|
\end{aligned}$$

there are twelve different cases:

$$\begin{aligned}
\text{1a:}\ \underline{\Psi}_{S,1<<} &= \underline{\Psi}_0(R_1) + \underline{Q}_1\underline{\Psi}_0(R_2) + (\underline{Q}_2 - \underline{Q}_1)\,\underline{\Psi}_{S1+} + (\underline{Q}_3 - \underline{Q}_2)\,\underline{\Psi}_{S2+} \\
\text{1b:}\ \underline{\Psi}_{S,1<>} &= \underline{\Psi}_0(R_1) + \underline{Q}_1\underline{\Psi}_0(R_2) + (\underline{Q}_2 - \underline{Q}_1)\,\underline{\Psi}_{S1+} - (\underline{Q}_3 - \underline{Q}_2)\,\underline{\Psi}_{S2-} \\
\text{1c:}\ \underline{\Psi}_{S,1><} &= \underline{\Psi}_0(R_1) + \underline{Q}_1\underline{\Psi}_0(R_2) - (\underline{Q}_2 - \underline{Q}_1)\,\underline{\Psi}_{S1-} + (\underline{Q}_3 - \underline{Q}_2)\,\underline{\Psi}_{S2+} \\
\text{1d:}\ \underline{\Psi}_{S,1>>} &= \underline{\Psi}_0(R_1) + \underline{Q}_1\underline{\Psi}_0(R_2) - (\underline{Q}_2 - \underline{Q}_1)\,\underline{\Psi}_{S1-} - (\underline{Q}_3 - \underline{Q}_2)\,\underline{\Psi}_{S2-} \\
\text{2a:}\ \underline{\Psi}_{S,2<<} &= \underline{\Psi}_0(R_1) + \underline{Q}_2\underline{\Psi}_0(R_2) + (\underline{Q}_2 - \underline{Q}_1)\,\underline{\Psi}_{S1-} + (\underline{Q}_3 - \underline{Q}_2)\,\underline{\Psi}_{S2+} \\
\text{2b:}\ \underline{\Psi}_{S,2<>} &= \underline{\Psi}_0(R_1) + \underline{Q}_2\underline{\Psi}_0(R_2) + (\underline{Q}_2 - \underline{Q}_1)\,\underline{\Psi}_{S1-} - (\underline{Q}_3 - \underline{Q}_2)\,\underline{\Psi}_{S2-} \\
\text{2c:}\ \underline{\Psi}_{S,2><} &= \underline{\Psi}_0(R_1) + \underline{Q}_2\underline{\Psi}_0(R_2) + (\underline{Q}_2 - \underline{Q}_1)\,\underline{\Psi}_{S1+} + (\underline{Q}_3 - \underline{Q}_2)\,\underline{\Psi}_{S2+} \\
\text{2d:}\ \underline{\Psi}_{S,2>>} &= \underline{\Psi}_0(R_1) + \underline{Q}_2\underline{\Psi}_0(R_2) + (\underline{Q}_2 - \underline{Q}_1)\,\underline{\Psi}_{S1-} - (\underline{Q}_3 - \underline{Q}_2)\,\underline{\Psi}_{S2-} \\
\text{3a:}\ \underline{\Psi}_{S,3<<} &= \underline{\Psi}_0(R_1) + \underline{Q}_3\underline{\Psi}_0(R_2) + (\underline{Q}_2 - \underline{Q}_1)\,\underline{\Psi}_{S1-} + (\underline{Q}_3 - \underline{Q}_2)\,\underline{\Psi}_{S2-} \\
\text{3b:}\ \underline{\Psi}_{S,3<>} &= \underline{\Psi}_0(R_1) + \underline{Q}_3\underline{\Psi}_0(R_2) + (\underline{Q}_2 - \underline{Q}_1)\,\underline{\Psi}_{S1-} + (\underline{Q}_3 - \underline{Q}_2)\,\underline{\Psi}_{S2+} \\
\text{3c:}\ \underline{\Psi}_{S,3><} &= \underline{\Psi}_0(R_1) + \underline{Q}_3\underline{\Psi}_0(R_2) + (\underline{Q}_2 - \underline{Q}_1)\,\underline{\Psi}_{S1+} + (\underline{Q}_3 - \underline{Q}_2)\,\underline{\Psi}_{S2-} \\
\text{3d:}\ \underline{\Psi}_{S,3>>} &= \underline{\Psi}_0(R_1) + \underline{Q}_3\underline{\Psi}_0(R_2) + (\underline{Q}_2 - \underline{Q}_1)\,\underline{\Psi}_{S1+} + (\underline{Q}_3 - \underline{Q}_2)\,\underline{\Psi}_{S2+}
\end{aligned}$$

3 Simulation

The equations of the models without, with one and with two impedance jumps were coded in Python. The verification of the model without a jump was done by comparison with analytical results for simple configurations like e.g. a single sound source on hard ground.

The verification of the computer code for one jump was done by comparison with the transfer grid method developed by Rasmussen [7]. In this method the radiation from the source is received at 20 000 grid points in a plane above the impedance jump. All these points are acting as sources, radiating the sound to the receiver at the other side of the impedance jump.

In Figure 7 the differences in sound level between transfer grid method and de Jong model for one impedance jump at 1 kHz are displayed for distances from 5 to 50 m and for heights from 1 to 5 m. The source height is

positioned 0.5 m above the origin. The impedance of the plane in front of the jump is of class ”G” and behind the jump at a distance of 2 m of class ”C” like in Figure 5.

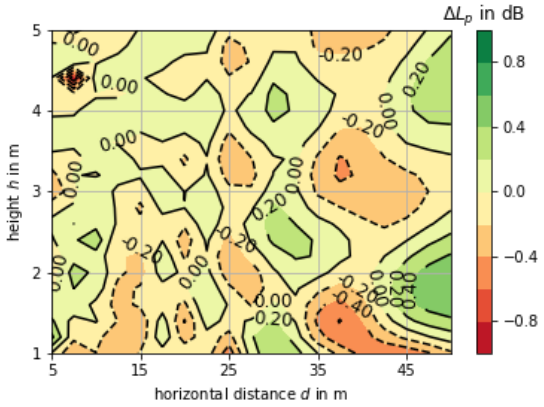

Figure 7: Differences in sound level for the simulation models with one jump at 1 kHz

In the simulation of the transfer grid method 200 points in width and 100 points in height were used. The grid constant was set to 0.2 times the wavelength. Hence the dimensions of the grid plan were about 10 m by 6 m.

The level differences are almost in a range of $\pm$ 0.2 dB except the area near the ground far away from the source and one small spot very high above the source, where strong interferences occur.

The model for two jumps was verified by using the same admittance on both sides of one of the jumps and comparing the results with the ones obtained by the model with one jump.

3.1. Description of the Model

The geometry of the simulation model for comparison with measurements, explained in the next section, is shown in Figure 8.

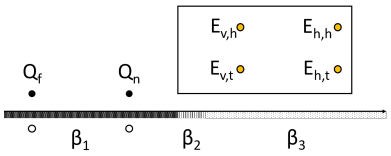

Figure 8: Geometry for sound propagation over a plane with one or two impedance jumps; comparison with measurements

The sound source, a passenger car, was located far ”Q_f” or near ”Q_n” the impedance jump. The admittance area before the jumps is denoted as ”β_1”, between the jumps as ”β_2” and after the jumps as ”β_3”. With ”$E_{v,t}$”, ”$E_{v,h}$”, ”$E_{h,t}$” and ”$E_{h,h}$” the microphone positions ”ahead” (v), ”behind” (h) and ”low” (t), ”high” (h) are marked, respectively.

3.2. Measurements

The acoustic effectiveness of two diffractor types was determined by means of controlled and statistical pass-by measurements. In order to ensure the best possible quantification of the noise reduction potential, the measurements were carried out on two times four microphones, simultaneously at the diffractor and at a reference. For comparison with simulations only the maximum sound levels from controlled pass-by measurements at Twente Airport near Enschede where used, because of the flat terrain there. For details see Strigari [10].

3.3. Comparison with measurements

The admittance for the stripe between the jumps, β_2, is not known. But from measurements with and without the stripe at the four microphone positions, the values for different frequency bands can be determined. For this purpose, simulations with different values for the admittance of the strip were conducted for all third octave bands. To compare the results with the measurements at the four microphone positions, the results of different frequencies were added up energetically.

In Figure 9 the comparison simulations for different admittances at the strip for the third octave band of 1 kHz are shown.

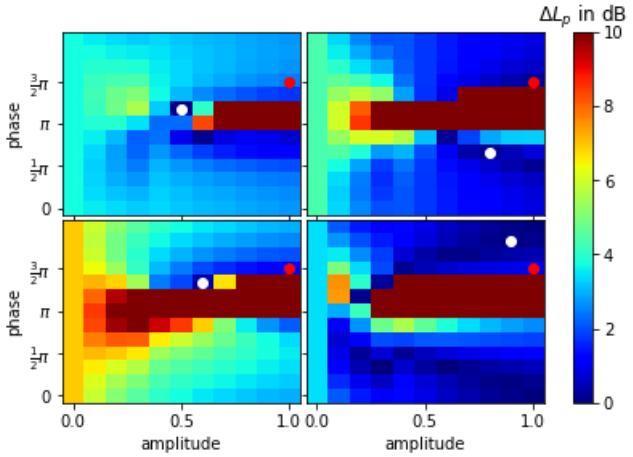

Figure 9: Comparison of four measurements with simulations for different admittances at the strip for the third octave band of 1 kHz

The complex admittance of the strip is parametrised with its two polar coordinates in the complex plane, the phase from 0 to 2π and the amplitude from 0 to 1. The level differences between simulation and measurements for the four microphone positions are shown in Figure 8. The individual minimum is marked by a white dot, the overall minimum for all positions together by a red dot. In this way for all third octave bands the parameters for an optimal fit were calculated. In Figure 10 the obtained parameter are displayed as normalised admittances (cyan lines) together with the ones for impedance classes ”C” and ”G” of NORD2000.

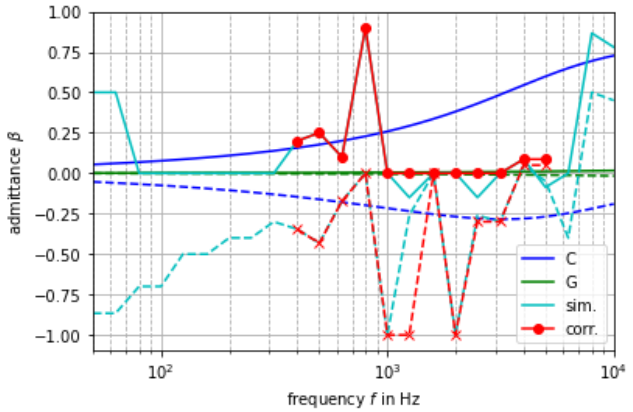

Figure 10: normalised admittance for impedance classes ”C” and ”G” of NORD2000 and for the simulation depending on frequency; solid line: real part, dashed line: imaginary part

There are some strange effects visible due to uncertainties in measurements and fitting process. These where corrected (red lines). Fore some frequencies, the results are even not jet satisfying.

3.4. Long range propagation

With the parameters of the normalised admittance β, obtained within the comparison of measurements and simulations, it is possible to calculate the long-range sound level.

The total level calculation from the third octave sound pressure levels $L_{p,i}$ was done with the normalised traffic noise spectrum [11] $\Delta L_{p,i}$ of third octave bands i:

$$L_t = 10 \lg \left[\sum_i 10^{0.1(L_{p,i} + \Delta L_{p,i})} \right] \tag{12}$$

From the difference of simulation with and without the diffractor the total noise reduction ΔL_p for the whole spectrum can be found. The calculation starts from 400 Hz and some third octave bands, namely 1250, 2500 and 5000 Hz were left out for reasons of faulty simulation results.

In Figure 11 the difference in total level ΔL_p is calculated for distances from 5 to 50 m and for heights from 1 to 5 m. In this case the diffractor had a width of 1 m and was placed 1.65 m from the near lane of the road, positioned at a distance of 0 m with a height of 0.5 m.

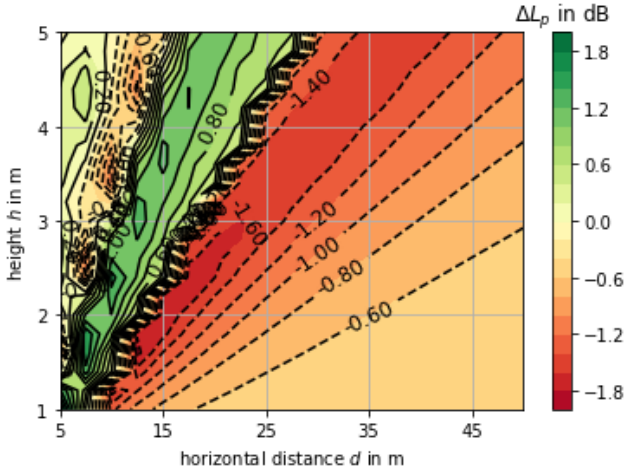

Figure 11: Total sound level difference for a diffractor of 1 m width for the near lane

The noise reduction is up to 2 dB for a sector with an angle of about 7° away from the sound source.

4 Conclusions

It is possible to simulate the noise propagation over impedance jumps with a set of compact mathematical formulations. This can used as a tool to integrate new noise abatement measures with physical frequency-dependant behaviour into engineering models of sound propagation like ISO 9613-2. The way to do this is using analogous frequency-dependant models for sources and barriers.

The noise reduction for WHIS®stone found near the road is conserved at greater distances. The research about acoustical effectiveness will continue, also for the products WHIS®wall and WHIS®top.

Acknowledgements

I would like to thank the company 4Silence for the kind admission at their headquarter on Twente airport and giving us the possibility for measurements at their site.

References

[1] Ministerie van Binnenlandse Zaken en Koninkrijksrelaties. Regeling van de staatssecretaris van infrastructuur en waterstaat en de minister van binnenlandse zaken en koninkrijksrelaties van 19 maart 2021 tot wijziging van de omgevingsregeling vanwege het opnemen van regels met het oog op de beheersing van geluid afkomstig van wegen, spoorwegen en industrieterreinen (aanvullingsregeling geluid omgevingswet), mar 2021. URL https://zoek.officielebekendmakingen.nl/stcrt-2021-15868.html#volgtOpmain_reg0001_d3088e1_cmp_IVA.

[2] ISO 9613-2. Acoustics - attenuation of sound during propagation outdoors - part 2: General method of calculation, December 1996.

[3] B. Plovsing and J. Kragh. Comprehensive outdoor sound propagation model. part 1: Propagation in an atmosphere without significant refraction. Technical report, DELTA, Danish Electronics, Light & Acoustics, Lyngby, 2001.

[4] *NT ACOU 104 - Ground surfaces: Determination of the acoustic impedance*, 1999.

[5] G. Taraldsen. The delany-bazley impedance model and darcy's law. *Acta Acust united Ac*, 91:4150–4165, 2005.

[6] M. A. Nobile and S. I Hayek. Acoustic propagation over an impedance plane. *J. Acoust. Soc. Am.*, 78(4): 1325–1336, 1985.

[7] K. B. Rasmussen. Propagation of road traffic noise over level terrain. *J. Sound Vib.*, 82(1):51–61, 1982.

[8] B. A. de Jong. Reekenmodellen om de invloed te voorspellen van en asfalt-grasovergang en van afscherming van een wal. Technical report, Technical University of Delft, Laboratorium voor Technische Natuurkunde, 1978.

[9] D. C. Hothersal and J. N. B. Harriott. Approximation models for sound propagation above multi-impedance plane boundaries. *J. Acoust. Soc. Am.*, 97(2):918–926, 1985.

[10] F. Strigari, R. Becker, and W. Bartolomaeus. Measurement of the acoustic effectiveness of diffractors. In *Euregio / BNAM2022*, 2022.

[11] EN 1793-3. Road traffic noise reducing devices - test method for determining the acoustic performance - part 3: Normalised traffic noise spectrum, November 1997.